



ISTITUTO NAZIONALE DI RICERCA METROLOGICA Repository Istituzionale

Sprayable Ultrablack Coating Based on Hollow Carbon Nanospheres

This is the author's accepted version of the contribution published as:

Original

Sprayable Ultrablack Coating Based on Hollow Carbon Nanospheres / Hu, Yuefan; Cao, Kangli; Rong, Hao; Xu, Jun; Han, Hexiang; Wang, Huifen; Pattelli, Lorenzo; Li, Na; Xu, Hongbo; Zhao, Jiupeng; Pan, Lei; Kuchmizhak, Aleksandr; Li, Yao. - In: ACS APPLIED NANO MATERIALS. - ISSN 2574-0970. - 4:8(2021), pp. 7995-8002. [10.1021/acsanm.1c01291]

Availability:

This version is available at: 11696/71402 since: 2021-10-11T23:33:51Z

Publisher:

ACS Publications

Published

DOI:10.1021/acsanm.1c01291

Terms of use:

This article is made available under terms and conditions as specified in the corresponding bibliographic description in the repository

Publisher copyright

American Chemical Society (ACS)

Copyright © American Chemical Society after peer review and after technical editing by the publisher. To access the final edited and published work see the DOI above.

(Article begins on next page)

Sprayable Ultra-Black Coating Based on Hollow Carbon Nanospheres

Yuefan Hu,^a Kangli Cao,^b Hao Rong,^a Jun Xu,^b Hexiang Han,^b Huifen Wang,^b Lorenzo Pattelli,

^{d,e} Na Li,^a Hongbo Xu,^a Jiupeng Zhao,^a Lei Pan,^{a,} Aleksandr Kuchmizhak,^{f,g,*} and Yao Li^{c,*}*

^a MIIT Key Laboratory of Critical Materials Technology for New Energy Conversion and

Storage, School of Chemistry and Chemical Engineering, Harbin Institute of Technology,

Harbin, 150001, P. R. China

^b Shanghai Institute of Spacecraft Equipment, Shanghai, 200240, P. R. China

^c National Key Laboratory of Science and Technology on Advanced Composites in Special

Environments, Harbin Institute of Technology, Harbin, 150001, China

^d European Laboratory for Non-linear Spectroscopy (LENS), Università di Firenze, Sesto

Fiorentino 50019, Italy

^e Istituto Nazionale di Ricerca Metrologica (INRiM), 10135 Turin, Italy

1
2
3
4 ^f Institute for Automation and Control Processes, Far Eastern Branch, Russian Academy of
5
6
7 Sciences, Vladivostok 690041, Russian Federation
8
9

10
11 ^g Far Eastern Federal University, Vladivostok 690922, Russia
12
13

14
15
16 Keywords: high absorption coatings; hollow carbon spheres; solar absorptance; adhesion;
17
18
19 hierarchical structure
20
21
22

23
24 ABSTRACT: Inexpensive, easy-to-implement coatings exhibiting extremely low reflectance
25
26
27 within a broad spectral range and good adhesion to substrates are in high demand for high-
28
29
30 precision optical instruments and solar energy harvesting. Herein, we demonstrate a highly
31
32
33 absorbing coating based on hollow carbon nanospheres (HCSs). The coatings are formed via a
34
35
36 simple and high-performing air-spraying process with a tailored paint formulation containing
37
38
39 HCSs as an absorbing pigment and a fluororesin as a binder. By optimizing the pigment/binder
40
41
42 mass ratio (P/B), we produce functional coatings that exhibit solar absorptance up to 0.985 and
43
44
45 good adhesion to aluminum sheets of grade 2 (according to the ISO 2409 standard). The excellent
46
47
48 solar absorptance of the obtained coatings results from their hierarchical nano- and micro-scale
49
50
51 surface morphology, providing a refractive index gradient on the air-coating interface as well as
52
53
54
55
56
57
58
59
60

1
2
3 remarkable light trapping performance. The former is due to the hollow structure in carbon spheres,
4
5
6
7 which is preserved after the addition of the binder because the size of binder particles is larger than
8
9
10 the holes on the shell of the HCSs. The latter is attributed to the micro-nodules and micro-pits of
11
12
13 the coating surface formed by the agglomeration of the HCSs, which enhances absorption by
14
15
16
17 multiple scattering.
18
19
20
21

22 **1. Introduction**

23
24

25 As predicted by Snell's law, reflection occurring at the air-solid interface is inevitable due to the
26
27
28 presence of a refractive index discontinuity. Unwanted reflections are detrimental for many
29
30
31 applications such as high-performance optical devices or solar energy collectors.^{1,2} In these cases,
32
33
34 "ultra-black" surfaces possessing extremely low reflectance over a broad spectral range are highly
35
36
37
38 demanded.
39
40
41

42 Numerous studies were undertaken to minimize the surface reflection.^{3,4} In general, three basic
43
44
45 principles, operating independently or simultaneously,⁵ have been employed to form a natural^{6, 7}
46
47
48 or artificially designed low-reflectivity surface in these studies:
49
50
51

52 (1) Formation of large (as compared to the wavelength) nodules or pits to trap incident light via
53
54
55 multiple reflections and absorptions within the surface;⁸⁻¹⁵
56
57
58
59
60

1
2
3
4 (2) Incorporation of low-density surface layers to produce a gradual variation of the refractive
5
6
7 index, suppressing Fresnel reflection;^{9,15-23}
8
9

10 (3) Use of noble-metal or high-refractive-index nanoparticles to achieve efficient broadband
11
12
13 solar absorption via bandgap engineering or by coupling to either surface plasmons or Mie-type
14
15
16 resonances.^{4,24-27}
17
18
19

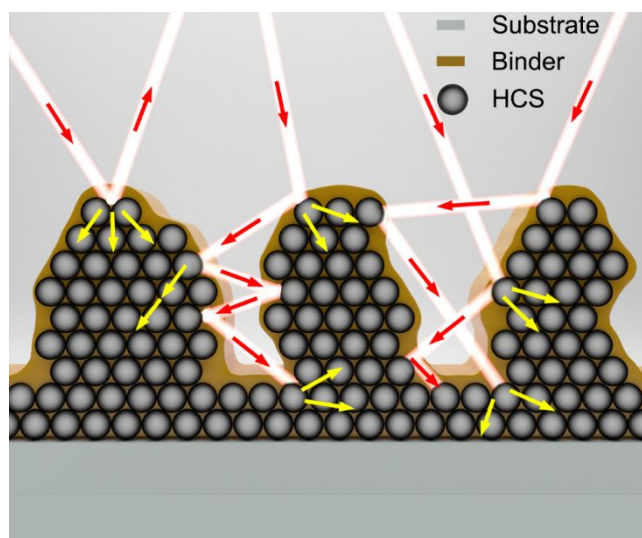
20 Carbon is the most commonly used absorber for black paints due to its low price and wide
21
22
23 absorption band. Carbon-based materials with low density such as carbon nanotubes have been
24
25
26 widely employed as ultra-black materials for high-end optical applications. Yang et al. obtained
27
28
29 an extremely low reflectance (lower than 0.07%) within a visible wavelength range of 457-633 nm
30
31
32 using arrays of aligned nanotubes produced by a chemical vapor deposition.¹⁸ Zhu et al. fabricated
33
34
35 carbon aerogels via a supercritical drying method, which exhibited a total reflectance lower than
36
37
38 0.24% in a spectral range of 400-2000 nm.¹⁹ Mentioned materials demonstrated an excellent light-
39
40
41 absorbing performance due to multiple open pores, which decrease the refractive index jump at
42
43
44 the air interface. However, the produced coatings typically had weak adhesion to a substrate or
45
46
47 were prepared in the form of a self-supporting membrane, thus limiting their practical applicability.
48
49
50

51 To improve the adhesion of the nanotube-based coatings, Magdassi et al. mixed multi-walled
52
53
54
55
56
57
58
59
60

1
2
3 carbon nanotubes with a silicone, then the mixture was sprayed on an aluminum substrate to obtain
4
5
6
7 the ultra-black coating.²⁸⁻³⁰ The resulting adhesion was significantly improved, but at the cost of a
8
9
10 substantial increase of average reflectance up to 2-5%, i.e. to a level that is not acceptable for
11
12
13 certain applications. Similar result is reported for carbon aerogels³¹ too. This is due to the fact that
14
15
16 the binder infiltrates the gaps between the nanotubes potentially penetrating into the nanotubes, as
17
18
19 well. Negative contribution of the binder can be mitigated by reducing its concentration, for
20
21
22 example, by using tightly packed nanoparticles or introducing empty closed-cell pores³² to obtain
23
24
25 a smoother refractive index transition at the air-coating interface.
26
27
28
29

30 In this study, we report the fabrication of ultra-black coatings based on hollow carbon
31
32
33 nanospheres (HCSs), which were chosen as an absorbing pigment according to the following
34
35
36 reasons. First of all, the hollow structure of the nanospheres reduces the overall density and average
37
38
39 refractive index of the resulting coatings. Second, the agglomerated HCSs create a disordered
40
41
42 micro-scale surface morphology that facilitates light trapping and reduces inter-particle gaps,
43
44
45 decreasing the binder consumption. Figure 1 schematically illustrates the general structure of the
46
47
48 proposed HCS-based coating. The agglomerated hollow spheres form micron-sized surface
49
50
51 nodules and pits wrapped by a thin binder layer which fills the inter-particle gaps, while the hollow
52
53
54
55
56
57
58
59
60

1
2
3 core remains intact. When light irradiates such a hierarchical surface, reflection is substantially
4
5
6
7 suppressed via light trapping and decreased Fresnel reflection.
8
9



10
11
12
13
14
15
16
17
18
19
20
21
22
23
24
25
26
27
28
29 Figure 1. Schematic of the proposed HCS-based coating. The incident light rays in the air are
30
31
32 shown by red arrows, while the yellow ones indicate the radiation trapped by the HCSs.
33
34
35
36
37
38

39 2. Experimental Section/Methods

40 2.1 Chemicals and materials

41
42
43 Analytical grade reagents including ammonia, ethyl alcohol, resorcinol, formaldehyde,
44
45
46
47
48
49 cetyltrimethylammonium bromide (CTAB), hydrofluoric acid and acetone were purchased from
50
51
52
53 Sigma-Aldrich and used without further purification. Poly(vinylidene fluoride-co-

chlorotrifluoroethylene) was purchased from HWRK CHEM (China) and used as a binder. Tetraethyl orthosilicate (TEOS) was distilled before use. Ultra-pure water was obtained from an in-house filtration system (CSR-1-30T).

2.2 Preparation of HCSs

HCSs were synthesized according to the methods described in the literature.³³⁻³⁵ The process involves four steps: (1) the synthesis of SiO₂ spherical particles, (2) their coating by the resorcinol formaldehyde resin (RF resin), (3) carbonization of SiO₂@RF spheres, and (4) the removal of the remaining SiO₂ via etching (Figure 2).

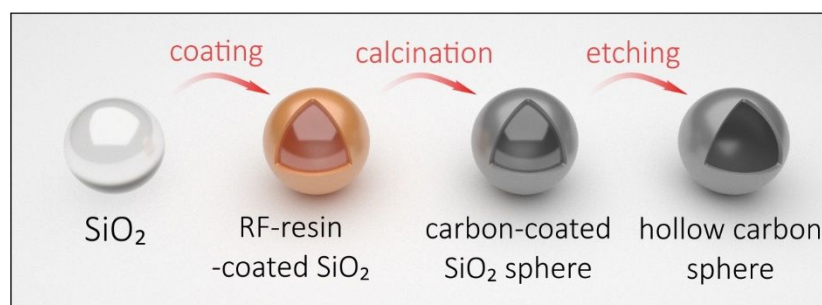


Figure 2. Schematic of the HCS synthesis

(1) Synthesis of silica microspheres as a sacrificial template. First, 22 mL water, 150 mL ethanol, and 9 mL ammonium solution (14 mol/L) were mixed in a 500 mL reactor in a water bath at 40°C and vigorously stirred for 5 min. Then, 5 g TEOS and 20 ml ethyl alcohol were added into the

1
2
3 reactor. A colloidal solution of SiO₂ nanospheres with a diameter of approximately 150~200 nm
4
5
6
7 was obtained by maintaining the temperature and stirring for 8 h.
8
9

10 **(2) Synthesis of RF-resin-coated SiO₂ spheres.** 2 g of SiO₂ spheres were washed twice and mixed
11
12
13 with 3 mL of ammonia solution (14 mol/L) and 20 mL of CTAB (0.01 mol/L) in 500 mL of water
14
15
16 in a 1L reactor, followed by stirring for 5 min. Subsequently, 2 g resorcinol and 25 mL (40%
17
18
19 volume) of formaldehyde solution were added in the reactor. The SiO₂@RF composite was
20
21
22
23 obtained after stirring at room temperature for 15 h.
24
25
26

27 **(3) Synthesis of carbon-coated SiO₂ spheres.** After a series of precipitation, washing and drying
28
29
30 steps, the SiO₂@RF composite was heated at 600 °C under an Ar atmosphere for 8 h to obtain the
31
32
33
34 clumped SiO₂@C.
35
36

37 **(4) Synthesis of hollow carbon sphere.** SiO₂@C was further ground into powder using a mortar.
38
39
40 Then, the powder was etched in HF solution under vigorous stirring to remove SiO₂, leaving only
41
42
43
44 the carbon shell. After drying, the HCSs was ground again to improve dispersion in the fluororesin
45
46
47
48 solution.
49

50 **2.3 Preparation of the HCS coating**

51
52
53
54
55
56
57
58
59
60

1
2
3
4 An aluminum sheet was roughened by sandpaper and used as a substrate for HCS-based
5
6
7 coatings. The typical roughness of the Al sheet assessed using optical profilometry was about 3
8
9
10 μm (Figure S1). The paint was prepared by mixing the HCSs with the fluoro-resin in acetone at
11
12
13 different ratios and sonicated for 10 min. Then the paint was uniformly sprayed onto the Al sheets
14
15
16
17 by an air spraying gun. Typically, spraying procedure was repeated several times to achieve
18
19
20 uniform coverage (see Supporting Information). Finally, the coatings were put at room temperature
21
22
23
24 for 30 min until complete solidification.

25 26 27 **2.4 Coating characterization**

28
29
30 The surface morphology of the produced coatings was studied by a field-emission scanning
31
32
33 electron microscope (Hitachi SU 8010) and transmission electron microscope (Hitachi H-7650).
34
35
36
37 Reactive ion etching (RIE) of the HCS coatings was performed with a RIE apparatus (RIE-601)
38
39
40 using argon as the reactive gas, that allowed to etch both the HCSs and the fluoro-resin. Etching
41
42
43
44 depth was controlled by varying the etching time. The working power, reactor pressure and argon
45
46
47 flow rate were set to 150 W, 100 mtorr, and 30 sccm, respectively.

48
49
50 The solar absorptance, A_s , was calculated from the diffuse reflection spectra measured by the
51
52
53
54 Lambda 950 UV-visible spectrophotometer coupled to an integrating sphere. Since the coatings
55
56
57
58
59
60

1
2
3 were applied above the Al substrates, the total transmittance is zero ($T_s=0$), and the solar
4
5
6 absorptance can be assessed as:
7
8
9

$$10 \quad A_s = 1 - R_s \quad (1)$$

11
12 where R_s is the solar reflectance defined as the ratio between reflected and incident solar flux.
13
14

15
16 Reflectance of the HCS-based coatings was also modeled using finite-difference time-domain
17
18 (FDTD) calculations (Figure S2). The 5- μm thick coatings comprised of the randomly arranged
19
20 monodisperse HCSs with variable diameter and shell thickness were simulated. The simulation
21
22 volume was limited by periodic boundary conditions applied along both lateral directions as well
23
24 as perfect matched layers along vertical direction.
25
26
27
28
29
30
31
32

33
34 Nitrogen adsorption was used to estimate the pore size distribution and pore volume of materials
35
36 by measuring the amount of the gas condensed on the sample at variable pressure. The size of
37
38 fluorescein molecule was assessed using dynamic light scattering (DLS, Malvern Zetasizer nano
39
40 ZS90).
41
42
43
44
45

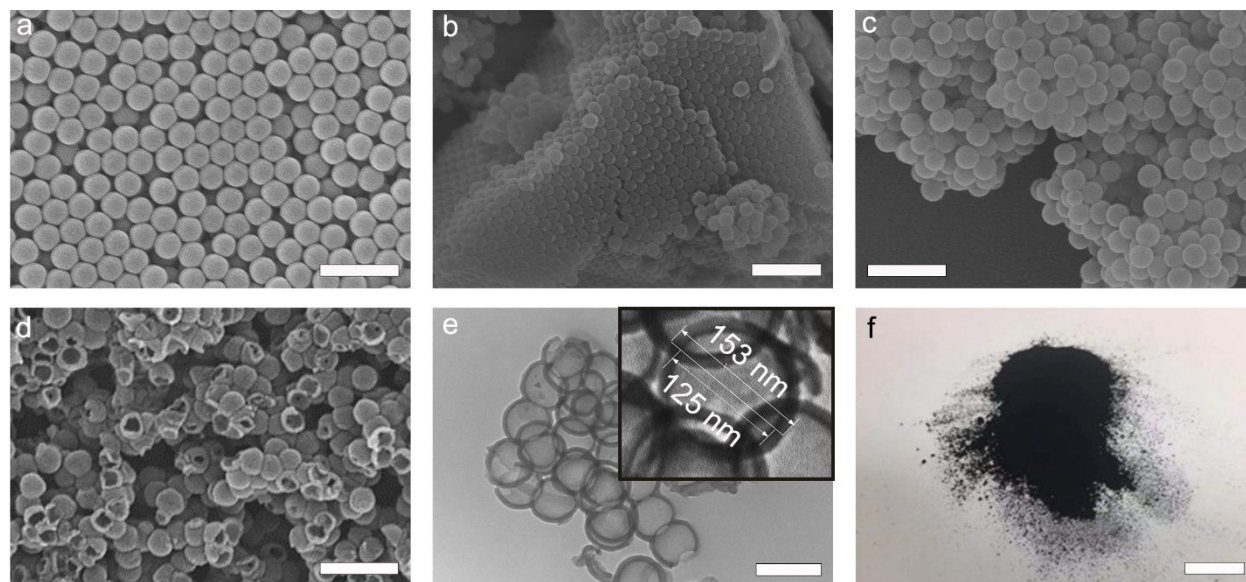
46
47 Adhesion of the HCS coatings was evaluated according to the ISO 2409 standard. Specifically,
48
49 HCS coatings were cut horizontally and vertically at a distance of 1 mm and stuck with a tape
50
51 several times to classify the fraction of detached material according to a standard scale.
52
53
54
55
56
57
58
59
60

3. Results and discussion

3.1 HCS-based coatings: key factors of high absorptance

As mentioned above, the synthesis of the HCSs involves four consecutive steps. Figure 3 demonstrates evolution of the morphologies of the SiO₂ nanospheres obtained at each step. It can be observed that the initial diameter of the SiO₂ nanospheres is approximately 170 nm (Figure 3a), which ensures the subwavelength size of the resulting HCS product. Figure 3b,c demonstrates the morphologies of the SiO₂@RF and SiO₂@C nanospheres, respectively. Both these products show partial agglomeration, leading to the formation of micron-sized surface features. SEM and TEM images of the final product reveal hollow structure of the carbon nanospheres, particularly owing to appearance of nanospheres with a broken shell (Figure 3d,e). The break of the shell may result from the grinding process of the partially agglomerated nanomaterial; however, the majority of the HCSs preserve unbroken shell. In this respect, the broken nanospheres are expected to weakly affect the optical properties of the resulting HCS-based coatings. Noteworthy, the average size of the HCSs reduces down to 153 nm with respect to 170-nm diameter pristine SiO₂ nanospheres. This is caused by the shrinkage of SiO₂³⁶ and the carbon sphere during the calcination process.

1
2
3
4 According to the performed TEM studies the thickness of the carbon shell is about 14 nm (Figure
5
6
7 3e, inset).
8
9



30
31
32
33
34
35
36
37
38
39
40
41
42
43
44
45
46
47
48
49
50
51
52
53
54
55
56
57
58
59
60

Figure 3. (a-d) Series of SEM images showing the evolution of the morphology of the SiO₂ microspheres on each consecutive fabrication step. (e) TEM image of the produced HCSs. Inset provides magnified view of representative nanosphere with the outer and inner diameters around 153 and 125 nm yielding in the corresponding average carbon shell thickness of 14 nm. (f) Optical image of the HCS-based powder. The scale bars in the images (a)-(f) correspond to 500 nm, 1 μ m, 500 nm, 500 nm, 200 nm, 2 cm respectively.

1
2
3
4 As recently reported by Guo *et al.*, HCSs as spherically symmetric structures exhibit geometry-
5
6
7 dependent scattering resonances that selectively enhance reflectance at certain wavelengths and
8
9
10 lead to conspicuous coloration of the HCS-based coatings.³⁷ However, our HCS powders appear
11
12
13 completely black (Figure 3f), which can be ascribed to the smaller size of the used nanospheres
14
15
16 with respect to those reported in ³⁷. This deduction was particularly confirmed by numerical
17
18
19 modeling of the reflectance spectra of the HCS-based coatings containing several layers of
20
21
22 randomly arranged HCSs with different diameters (Figure S2). As expected, the reflectance peaks
23
24
25 observed in the calculated spectra demonstrate systematic blueshift at decreasing diameter of the
26
27
28 HCSs, moving out of the solar wavelength range when the diameter of HCSs reaches 150 nm. As
29
30
31 we will show further, this is well consistent with the measured spectral response of the HCS-based
32
33
34 coatings. Therefore, in our case, the spherical symmetry of the used HCSs does not represent a
35
36
37 problem, allowing to obtain highly absorbing nanomaterial via simple synthesis procedure.
38
39
40
41 Noteworthy, utilization of the polydisperse HCSs can potentially solve the problem associated
42
43
44 with a structural color that comes from the spherical symmetry of the nanoparticles. For example,
45
46
47 this can be easily achieved by using TEOS with low purity. However, apart from expectedly low
48
49
50
51
52
53
54
55
56
57
58
59
60

1
2
3 reproducibility of the produced coatings, polydisperse HCSs cannot provide the densest
4
5
6
7 arrangement that will require more binder and result in higher reflectance of the produced coatings.
8
9

10 The paint solutions were prepared by mixing the HCSs with the fluororesin binder at different
11
12
13 mass ratio (P:B) and air-sprayed on the Al sheets. Noteworthy, the binder concentration strongly
14
15
16 affects the spraying process. At a specific P:B ratio, a lower binder concentration results in higher
17
18
19 amount of the used solvent and lower viscosity of the resulting solution. When the viscosity is too
20
21
22 low, the fluidity of the liquid drops on the Al sheet is too high, which is not conducive to the
23
24
25 formation of uniform coating, especially at the non-horizontal surface. However, if the viscosity
26
27
28 is too high, the risk of clogging of the spray gun increases. Therefore, we chose the range of the
29
30
31 binder concentrations at which spraying can be carried out safely. At such concentrations, because
32
33
34 the fluidity of the droplets is very low, spraying procedure are to be performed several times to
35
36
37 produce uniform HCS-based coating completely covering the Al sheet (Figure S3). The minimal
38
39
40 thickness of such uniform coating was assessed to be about 30 μm (Figure S4).
41
42
43
44
45
46

47 Integral reflectance R_s of the HCS-based coatings produced at different P/B ratio was
48
49
50 systematically measured across the wavelength range of 250-2500 nm. These measurements
51
52
53 showed that the coating reflectance increases with the binder content (Figure 4). More specifically,
54
55
56
57
58
59
60

1
2
3
4 when P/B is 1:10, the integral solar absorptance A_s is 0.963 ($R_s=0.037$), reaching 0.985 ($R_s=0.015$)
5
6
7 at P/B=1:2. Further decrease of the binder content leads to a visible reduction of the adhesion of
8
9
10 the produced coatings. The variation of the solar absorptance with the binder amount is associated
11
12
13 to a corresponding evolution of the morphology of the produced HCS-based coatings. In particular,
14
15
16
17 Figure 5a,b shows that the surface of the black coating produced at P/B of 1:10 exhibits rather
18
19
20 gentle protrusions insufficient to provide significant light trapping performance. Furthermore,
21
22
23
24 HCSs can hardly be identified beneath the coating surface, indicating an excessive amount of the
25
26
27 binder. This leads to an increased refractive index contrast at the air-coating interface. In contrast,
28
29
30 the rough surface of the coating produced at P/B of 1:2 is characterized by multiple micron-scale
31
32
33 pits made of agglomerated nanospheres where light can penetrate and undergo multiple scattering
34
35
36 and absorption events (see Figure 5c). A closer look at the surface morphology of such coating
37
38
39 shows agglomerated HCSs capped by a thin resin “skin” (Figure 5d), which favors suppression of
40
41
42
43 the Fresnel reflection and facilitates the absorption of the incident light. Both the rough surface
44
45
46 morphology and the relative increase of the pigment mass content contribute to the strong integral
47
48
49 absorptance of the HCS-based coatings produced at P/B = 1:2. In this respect, it is complicated to
50
51
52
53 assess contribution of both factors to the achieved low solar absorptance. Noteworthy, as it was
54
55
56
57
58
59
60

mentioned above, the minimal thickness of the uniform HCS-based coating was about 30 μm .

Further increase of the coating thickness provided no evident improvement of the integral solar

absorptance, while required excessive usage of the nanomaterial and chemicals.

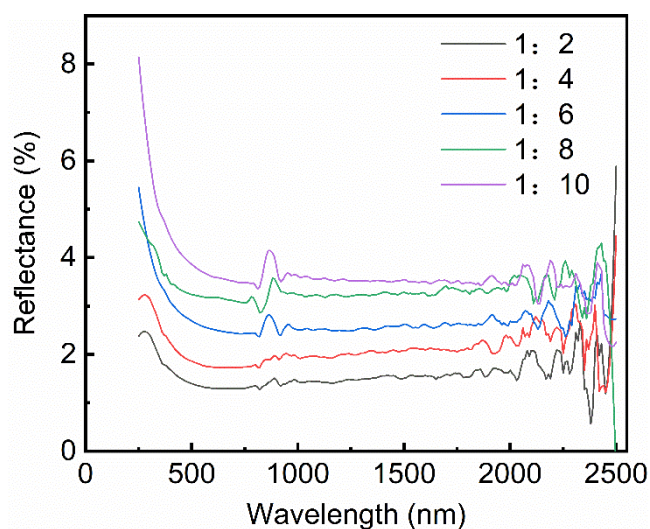
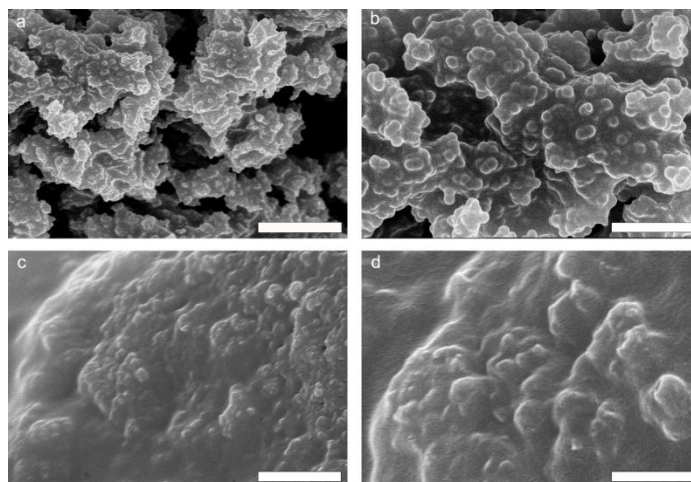


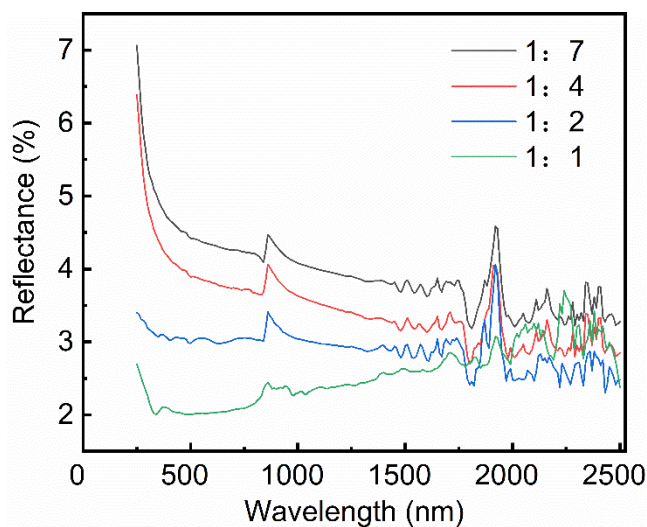
Figure 4. Reflectance spectra of the HCS-based coatings produced at different P/B mass ratio.



1
2
3
4 Figure 5. SEM images illustrating morphology of the HCS-based coatings with a P/B ration of 1:2
5
6
7 (a,b) and 1:10 (c,d). The scale bars correspond to 5 μm in (a,c), and 500 nm in (b,d).
8
9

10
11
12
13 To clarify the effect of the hollow microsphere geometry on the absorption characteristics of the
14 HCS-based paints, we fabricated and tested the additional type of coating made of solid carbon
15
16
17 sphere (SCS) mixed with a binder at similar P/B ratio (see Figure S5). Similarly to the HCS-based
18
19
20 coatings, the averaged reflectance of the SCS-based coatings increases at elevated binder content
21
22
23 as it is illustrated in Figure 6. The strongest solar absorptance of 0.978 ($R_s=0.022$) was achieved
24
25
26 at P/B ratio of 1:1. Noteworthy, such coating possesses physical characteristics and surface
27
28
29 morphology close to those for the HCS-based coating produced at P/B ratio of 1:2 (see Figure S6).
30
31
32
33 Meanwhile, difference in the achieved averaged reflectance for both coatings clearly reveals the
34
35
36 positive effect of the hollow morphology of the nanospheres on light-absorbing performance of
37
38
39 the resulting coating. At first glance, the difference between HCS- and SCS-based coatings may
40
41
42
43 seem insignificant; however, for certain applications as stray light suppression, such improvement
44
45
46
47 will play crucial role in resulting device performance. For example, when the stray light hits the
48
49
50
51
52
53
54
55
56
57
58
59
60

1
2
3
4 black-covered hood for 10 subsequent reflections, the HCS coating will provide 46-fold stronger
5
6
7 suppression of the reflected light intensity compared to that of the SCS-based coating.
8
9



10
11
12
13
14
15
16
17
18
19
20
21
22
23
24
25
26
27
28
29 Figure 6. Reflectance spectra of the SCS-based coatings produced at different P/B ratio.
30
31
32

33 3.2 Preservation of hollow morphology of the nanospheres mixed with a binder

34
35
36 To ensure the highest absorption, the HCSs must preserve hollow morphology when mixed with
37
38 a binder to produce the ultra-black coating. However, the fluororesin can potentially penetrate
39
40 inside the HCSs through the nanopores formed in the carbon shell of the HCSs during calcination
41
42 process (Figure 2). RIE procedure was first carried out to reveal internal structure of the HCSs in
43
44 the produced coatings. The surface morphology of the HCS-based coating (with P/B ratio of 1:2)
45
46
47 etched at different depths by varying exposure time from 2 to 10 min is illustrated by a series of
48
49
50
51
52
53
54
55
56
57
58
59
60

SEM images in Figure 7. As can be seen, no visible blockage is detected inside the isolated HCSs visualized at different etching stages confirming impermeability of the carbon shells.

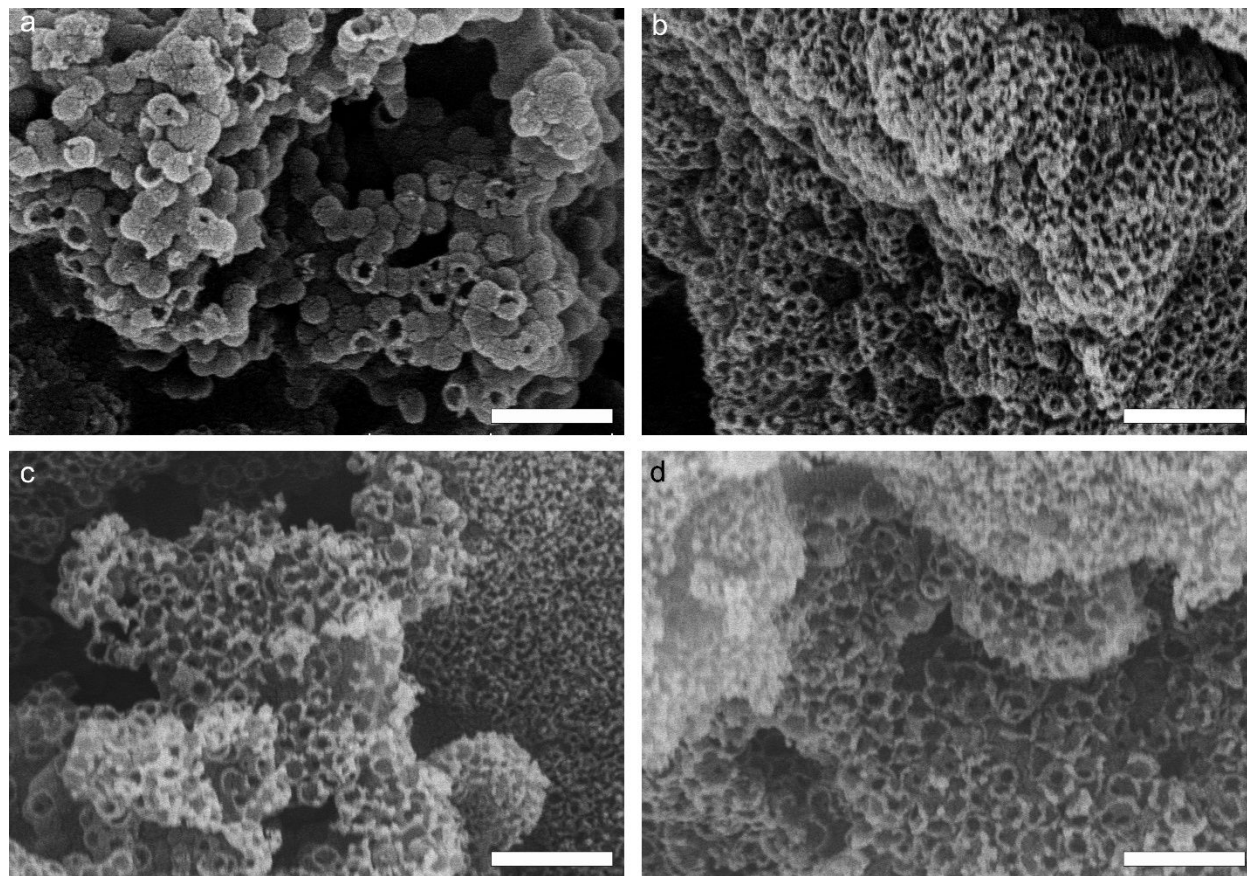


Figure 7. Series of SEM images showing surface morphology of the HCS-based coatings after their reactive ion etching at different etching time: 2 min (a), 4 min (b), 6 min (c) and 10 min (d). The scale bars are 500 nm for all images.

To further explore why fluorescein does not penetrate into the HCSs, the distribution of the pore size in the carbon shell were examined using nitrogen adsorption method. The N_2 adsorption-

1
2
3
4 desorption isotherms of the HCSs (Figure 8a) shows a sharp capillary condensation at high partial
5
6
7 pressure ($p/p_0=0.91-0.99$; p is the pressure at equilibrium, p_0 is the saturated vapor pressure) as
8
9
10 well as H1-type hysteresis loop, indicating a narrow pore size distribution. At low partial pressure
11
12
13 ($p/p_0<0.4$), the adsorption and desorption curves are very close, indicating the presence of the
14
15
16 multiple nanopores. The relationship between differential pore volume ($\Delta V/\Delta W$) and pore size
17
18
19 (W) was obtained through the Density Functional Theory. As shown in Figure 8b, the HCSs show
20
21
22 a bimodal pore distribution. The main maximum at 120.8 nm can be attributed to the hollow core
23
24
25 of the HCSs, while the second one (around 1 nm) – to the nanopores in the carbon shell.
26
27
28 Approximate size of the fluorescein particles was evaluated using DLS and Tyndall test (Figures
29
30
31 S7 and S8). DLS measurements indicated hydrodynamic feature size of the fluorescein of about
32
33
34 few hundred nanometers, that could correspond to one-dimensional size of the unfold fluorescein
35
36
37 chain. Distinct laser radiation path observed during the Tyndall test also confirmed similar
38
39
40 characteristic size of the fluorescein. The difference in the characteristic size of the shell nanopores
41
42
43 and the fluorescein apparently explains the impermeability of the carbon shell.
44
45
46
47
48
49
50
51
52
53
54
55
56
57
58
59
60

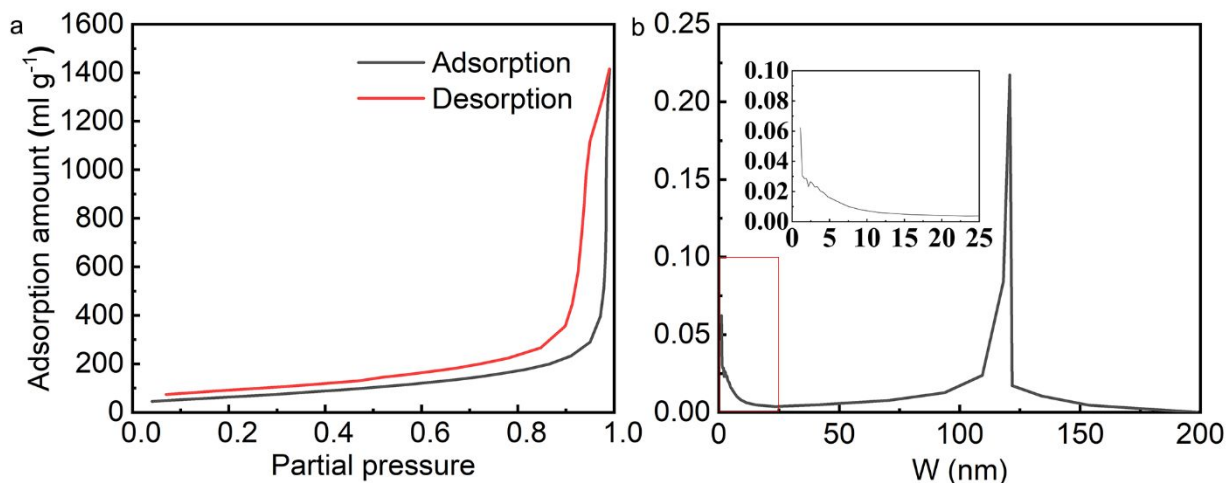


Figure 8. (a) Adsorption-desorption isotherm of nitrogen with respect to the HCS; (b) Differential pore volume $\Delta V/\Delta W$ as a function of the pore size W calculated by the Density Functional Theory.

Inset shows a magnified view of the red-square area.

3.3 Adhesion of the HCS-based coatings

The adhesion of the ultra-black coatings to the substrates is essential for practical applications. The adhesion of the HCS-based coatings produced at different P/B ratio was evaluated by the standard cross-cut tape test (ISO 2409). Figure 9 provides optical photograph of the coatings arranged on a black cloth after performing adhesion test. Reflectance spectrum of the black cloth is provided in Figure S9. As can be seen, the HCS-based coatings with high binder content (P/B ratio of 1:8 and 1:10) demonstrate remarkable adhesion characterized by small detached areas only

1
2
3 near the cut intersections. This results can be used to rate such coatings as grade 1. The coatings
4
5
6 produced at moderate P/B ratio of 1:6 and 1:4 shows detached areas not only at the intersection
7
8
9 but also along the cut edges. Nonetheless, the affected cross-cutting area was less than 15%, and
10
11
12 the adhesion of such coatings can be rated as grade 2. For HCS-based coatings with the highest
13
14
15 absorbance (P/B ratio of 1:2), their adhesion was rated as grade 3 according to the affected cross-
16
17
18 cutting area less than 35% making such coatings of practical interest as well. At even higher P/B
19
20
21 ratios, such as 1:1, the adhesion becomes too weak leading to large-area peeling of the coating
22
23
24
25
26 material even when it is subjected to slight scratches.
27
28
29
30
31
32
33
34
35
36
37
38
39
40
41
42
43
44
45
46
47
48
49
50
51
52
53
54
55
56
57
58
59
60

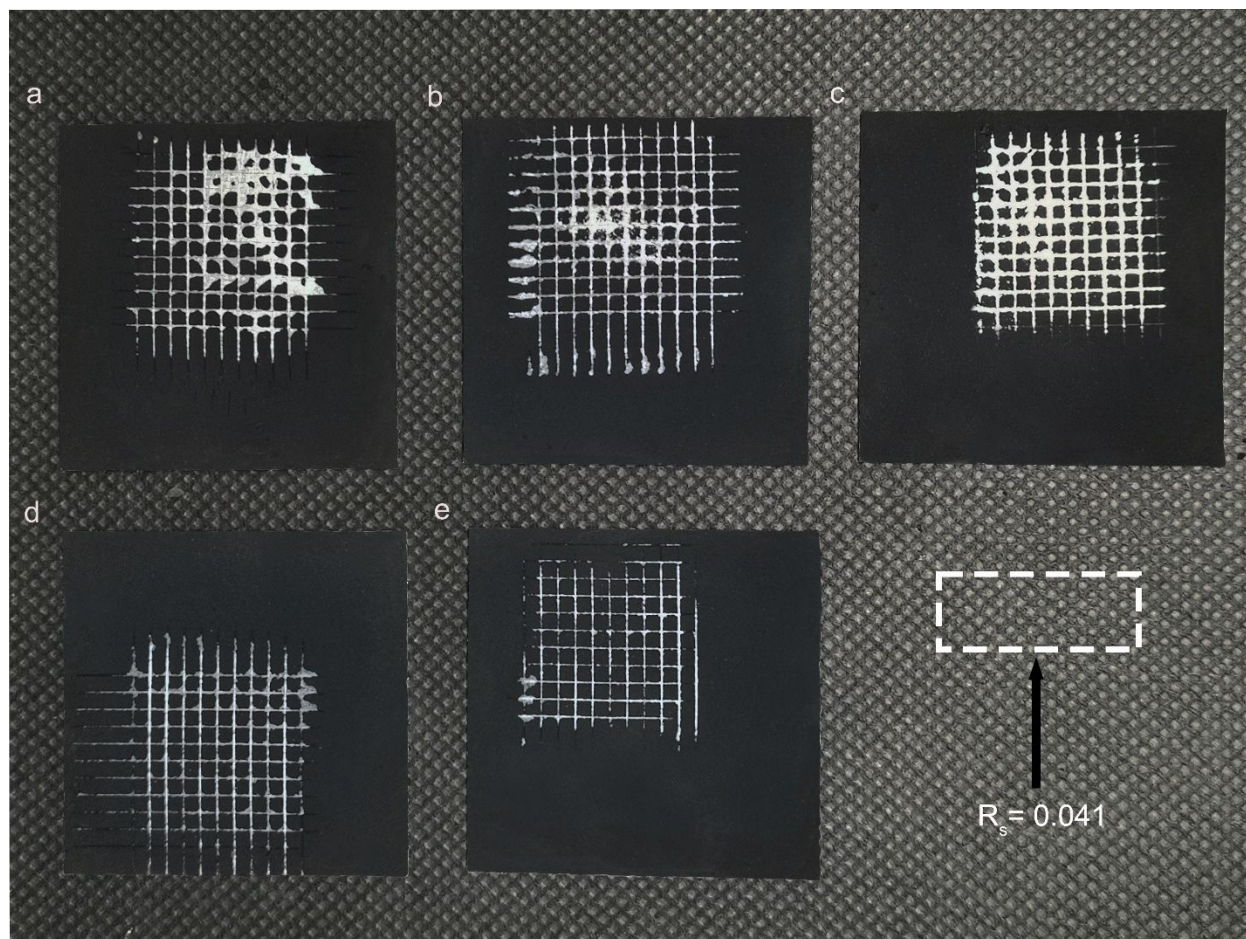


Figure 9. Digital images of the HCS-based coatings produced at different P/B ratio after performing the standard adhesion tests on a black paper. The black paper with solar reflectance of 0.041 is used as the background. The P/B ratio is (a) 1: 2; (b) 1:4; (c) 1:6; (d) 1:8; (e) 1:10. The length of a lattice with a white border is 2 mm.

Finally, to highlight the importance of the obtained results, we compare the main relevant characteristics of several reported state-of-the-art ultra-black carbon-based coatings with those

1
2
3 obtained for the developed HCSs-based coatings (Table 1). Pure (or binder-free) low-density
4
5
6 carbon-based materials typically provide integral absorption better than 0.99. However, these
7
8
9 characteristics decrease significantly (ca. 0.02) when the nanomaterial is mixed with the binder
10
11
12 that is required to achieve strong adhesion to the substrate in realistic applications.²⁸⁻³⁰ Similar idea
13
14
15
16 is clearly illustrated in Supporting Movie showing the reflectivity of He-Ne laser from several
17
18
19 ultra-black coatings. Conversely, the integral absorptance of the HCS-based coatings maintains a
20
21
22 high value of 0.985. This direct comparison indicated that the innovative HCS-based coatings
23
24
25
26 provide an excellent trade-off between strong broadband light absorption and good adhesion to the
27
28
29 substrate.
30
31
32
33
34
35
36

37 Table 1. The light absorption and adhesion performance of ultra-black carbon-based nanomaterials
38
39
40

			Optical property		Adding binder	Adhesion	Refs.
			spectrum range (nm)	integral absorptance			
Graphite composite	nanocone	nanowire	400-2000	ca 0.995	No	\	[16]
Hierarchical porous carbon spheres			300-2000	>0.997	No	\	[13]

Carbon aerogel	400-2000	>0.997	No	\	[19]
Carbon Vesicles	250-2000	>0.998	No	\	[37]
Carbon aerogel	400-1100	ca 0.98	Yes	grade 0	[31]
Multiwalled carbon nanotubes (MWCNT)	350-800	ca 0.973	Yes	grade 3	[28]
	850-2400	ca 0.961			
AlOOH/MWCNT	300-2500	ca 0.975	Yes	grade 1	[29]
Hollow carbon spheres	250-2500	0.985	Yes	grade 2 and 3	this work *

4. Conclusion

In this study, coatings with excellent solar absorptance were successfully fabricated by a simple and high-performing air-spraying process with a specially designed paint containing HCSs as a pigment and a fluoro-resin as a binder. By optimizing the pigment/binder ratio (P/B), a maximum solar absorptance of 0.985 was obtained at P/B of 1:2. Reactive ion etching proved the hollow nano-morphology of the HCSs that was preserved after the curing process. Tyndall effect, dynamic light scattering and nitrogen adsorption were used to assess and compare the typical size of the fluoro-resin particle and nanopore in the HCS shell explaining why the former can't penetrate inside the HCSs. The presence of hollow nanospheres allows to reduce the overall density of the coatings,

1
2
3 thus decreasing the Fresnel reflection, while the micro-scale surface morphology formed by the
4
5
6 agglomerated HCSs favors multiple reflections facilitating light absorption. In addition to
7
8
9 remarkable light absorption performance, good adhesion of the ultra-black coating to a substrate
10
11
12 is mandatory for practical application, which can be achieved by using a binder. However, the
13
14
15 addition of a binder typically causes a substantial increase of the averaged reflectance. In this work,
16
17
18 we have optimized the pigment/binder ratio and spraying procedure to achieve the coating
19
20
21 maintaining a strong absorbance combined with satisfactory good adhesion (grade 2 and 3
22
23 according to the ISO 2409 standard). Demonstrated characteristics make the produced HCS-based
24
25
26 coatings suitable for realistic applications such as solar energy harvesting, photothermal
27
28
29 conversion and designing of high-precision optical instruments. Moreover, the produced ultra-
30
31
32 black coatings possess rather low reflectance in the mid-IR spectral range (see Figure S10). This
33
34
35 indicates their high thermal emittance that is helpful for the temperature balance of the optical
36
37
38 instrument designed for space applications.
39
40
41
42
43
44
45

46
47 It should be stressed out that small amount of the hollow nanospheres appears to have a broken
48
49
50 shell after the grinding process. This can cause a certain increase of the reflectivity owing to
51
52
53 penetration of the binder inside the broken nanospheres. In this respect, further optimization of the
54
55
56
57
58
59
60

1
2
3 fabrication procedures can potentially improve light absorbing characteristics without reducing
4
5
6 adhesion performance. Nanospheres with more complicated multi-layer morphology can be also
7
8
9
10 considered as promising way to improved light absorption characteristics of the black paint^{15,38}.
11
12
13 However, additional studies are to be implemented to evaluate their matching with a binder to
14
15 realize coating with good adhesion. Such aspects as mixing ratio and potential penetration of
16
17 binder molecules inside the multi-layer nanospheres should be studied carefully to make the
18
19 decision regarding their capability to improve the already obtained characteristics. Other factors
20
21 as final price of the black paint and are also relevant for realistic applications.
22
23
24
25
26
27

28 ASSOCIATED CONTENT

30 31 32 **Supporting Information**

33
34
35
36 The following files are available free of charge.

37
38
39 Figure S1: Microtopography of the roughened Al sheet; Figure S2: Calculated reflectance of the
40
41
42 HCS-based coatings made of carbon nanospheres of variable outer diameter and shell thickness
43
44
45
46 Figure S3: Optical photograph of the HCS-based coatings produced by performing spraying
47
48
49 procedure several times; Figure S4: Side-view SEM images of the HCS-based coatings; Figure
50
51
52
53 S5: Comparative optical images of SCS- and HCS-based coatings; Figure S6: . Representative
54
55
56
57
58
59
60

1
2
3
4 SEM images demonstrating the surface morphology of the SCS-based coating; Figure S7:
5
6
7 Dynamic light scattering measurements of fluoresin; Figure S8: Tyndall effect in the
8
9
10 fluoresin solution; Figure S9: Reflection spectra of the black cloth; Figure S10: Reflectance of
11
12
13 ultra-black coating in thermal emittance band; Supplementary video comparing the He-Ne laser
14
15
16 reflection from different ultra-black coatings (MP4)
17
18
19
20
21
22

23 AUTHOR INFORMATION

24 25 26 **Corresponding Author**

27
28
29
30 **Lei Pan** — MIIT Key Laboratory of Critical Materials Technology for New Energy Conversion
31
32
33 and Storage, School of Chemistry and Chemical Engineering, Harbin Institute of Technology,
34
35
36 Harbin, 150001, P. R. China;

37
38
39
40
41 E-mail: panlei@hit.edu.cn
42
43
44

45 **Aleksandr Kuchmizhak** — Institute for Automation and Control Processes, Far Eastern Branch,
46
47
48 Russian Academy of Sciences, Vladivostok 690041, Russian Federation; Far Eastern Federal
49
50
51 University, Vladivostok 690922, Russia;

52
53
54
55 E-mail: alex.iacp.dvo@mail.ru
56
57
58
59
60

1
2
3 **Yao Li** — National Key Laboratory of Science and Technology on Advanced Composites in

4
5
6
7 Special Environments, Harbin Institute of Technology, Harbin, 150001, China;

8
9
10
11 E-mail: yaoli@hit.edu.cn

12
13
14
15 **Authors**

16
17
18
19 **Yuefan Hu, Hao Rong, Na Li, Hongbo Xu, Jiupeng Zhao** — MIIT Key Laboratory of Critical

20
21
22
23 Materials Technology for New Energy Conversion and Storage, School of Chemistry and

24
25
26
27 Chemical Engineering, Harbin Institute of Technology, Harbin, 150001, P. R. China

28
29
30
31 **Kangli Cao, Jun Xu, Hexiang Han, Huifen Wang** — Shanghai Institute of Spacecraft Equipment,

32
33
34
35 Shanghai, 200240, P. R. China

36
37
38 **Lorenzo Pattelli** — European Laboratory for Non-linear Spectroscopy (LENS), Università di

39
40
41
42 Firenze, Sesto Fiorentino 50019, Italy; Istituto Nazionale di Ricerca Metrologica (INRiM), 10135

43
44
45
46 Turin, Italy

47
48
49 **Notes**

50
51
52
53 The authors declare no competing financial interest.

54
55
56 **ACKNOWLEDGMENTS**

1
2
3
4 This work was supported by Shanghai Aerospace Science and Technology Innovation Fund
5
6
7 (SAST2017-065), Heilongjiang Provincial Postdoctoral Science Foundation (LBHZ-
8
9
10 15078, LBHZ-16080), China Postdoctoral Science Foundation (2016M601427) and National
11
12
13 Natural Science Foundation of China (No.51761135123, 52072096). A.K. expresses his gratitude
14
15
16 to the Ministry of Science and Higher Education of the Russian Federation (Grant Nos. MK-
17
18
19 4321.2021.1.2).

24 ABBREVIATIONS

25
26
27
28 HCS, hollow carbon sphere; P/B, pigment binder mass ratio; SCS, solid carbon sphere
29
30
31

32 REFERENCES

- 33
34
35
36 (1) Persky, M. J., Review of black surfaces for space-borne infrared systems. *Rev. Sci.*
37 *Instrum.* **1999**, 70, 2193-2217.
38
39 (2) Mccall, S. H. C. P.; Pompea, S. M.; Breault, R. P.; Regens, N. L., Reviews of Black
40 Surfaces for Space and Ground-Based Optical-Systems. In *Stray Radiation in Optical Systems*
41 *II 1993, Proceedings of the Society of Photo-Optical Instrumentation Engineers*, San Diego,
42 California, July 20-22, **1992**.
43
44 (3) Dou, S. L.; Xu, H. B.; Zhao, J. P.; Zhang, K.; Li, N.; Lin, Y. P.; Pan, L.; Li, Y.,
45 Bioinspired Microstructured Materials for Optical and Thermal Regulation. *Adv. Mater.* **2020**,
46 DIO:10.1002/adma.202000697.
47
48 (4) Huang, J. F.; Liu, C. X.; Zhu, Y. H.; Masala, S.; Alarousu, E.; Han, Y.; Fratolocchi, A.,
49 Harnessing structural darkness in the visible and infrared wavelengths for a new source of
50 light. *Nat. Nanotechnol* **2016**, 11, 60.
51
52
53
54
55
56
57
58
59
60

1
2
3
4 (5) Fan, P. X.; Bai, B. F.; Jin, G. F.; Zhang, H. J.; Zhong, M. L., Patternable fabrication of
5 hyper-hierarchical metal surface structures for ultrabroadband antireflection and self-cleaning.
6 *Appl. Surf. Sci.* **2018**, 457, 991-999.

7
8 (6) Niu, S. C.; Li, B.; Mu, Z. Z.; Yang, M.; Zhang, J. Q.; Han, Z. W.; Ren, L. Q., Excellent
9 structure-based multifunction of morpho butterfly wings: a review. *J. Bionic Eng.* **2015**, 12,
10 170-189.

11
12 (7) Han, Z. W.; Li, B.; Mu, Z. Z.; Yang, M.; Niu, S. C.; Zhang, J. Q.; Ren, L. Q., An
13 ingenious super light trapping surface templated from butterfly wing scales. *Nanoscale Res.*
14 *Lett.* **2015**, 10, 334.

15
16 (8) Han, Z. W.; Niu, S. C.; Li, W.; Ren, L. Q., Preparation of bionic nanostructures from
17 butterfly wings and their low reflectivity of ultraviolet. *Appl. Phys. Lett.* **2013**, 102,233702.

18
19 (9) Zhao, Q. B.; Fan, T. X.; Ding, J. A.; Zhang, D.; Guo, Q. X.; Kamada, M., Super black
20 and ultrathin amorphous carbon film inspired by anti-reflection architecture in butterfly wing.
21 *Carbon* **2011**, 49, 877-883.

22
23 (10) Fan, P. X.; Bai, B. F.; Zhong, M. L.; Zhang, H. J.; Long, J. Y.; Han, J. P.; Wang, W. Q.;
24 Jin, G. F., General Strategy toward Dual-Scale-Controlled Metallic Micro-Nano Hybrid
25 Structures with Ultralow Reflectance. *Acs Nano* **2017**, 11, 7401-7408.

26
27 (11) Yao, Z. P.; Hu, B.; Shen, Q. X.; Niu, A. X.; Jiang, Z. H.; Su, P. B.; Ju, P. F., Preparation
28 of black high absorbance and high emissivity thermal control coating on Ti alloy by plasma
29 electrolytic oxidation. *Surf. Coat. Tech.* **2014**, 253, 166-170.

30
31 (12) Xing, F.; Zhao, B. R.; Shi, W. Y., Study on tunable fabrication of the ultra-black Ni-P
32 film and its blacking mechanism. *Electrochim. Acta.* **2013**, 100, 157-163.

33
34 (13) Guo, J.; Li, D. D.; Zhao, H.; Zou, W. Z.; Yang, Z. S.; Qian, Z. C.; Yang, S. J.; Yang, M.;
35 Zhao, N.; Xu, J., Cast-and-Use Super Black Coating Based on Polymer-Derived Hierarchical
36 Porous Carbon Spheres. *Acs Appl. Mater. Inter.* **2019**, 11, 15945-15951.

37
38 (14) Xu, H. B.; Lu, N.; Qi, D. P.; Hao, J. Y.; Gao, L. G.; Zhang, B.; Chi, L. F., Biomimetic
39 Antireflective Si Nanopillar Arrays. *Small* **2008**, 4, 1972-1975.

40
41 (15) Carlesso, F.; Vieira, L. E. A.; Berni, L. A.; Savonov, G. d. S.; Oliva, A. R.; Finsterle,
42 W.; de Miranda, E. L., Physical and Optical Properties of Ultra-black Nickel-Phosphorus for a
43 Total Solar Irradiance Measurement. *Astrophysical Journal Supplement Series* **2020**, 248 (1).

1
2
3
4 (16) Sun, Y. R.; Evans, J.; Ding, F.; Liu, N.; Liu, W.; Zhang, Y.; He, S. L., Bendable, ultra-
5 black absorber based on a graphite nanocone nanowire composite structure. *Opt. Express*
6 **2015**, *23*, 20115-20123.

7
8 (17) Sun, C. H.; Jiang, P.; Jiang, B., Broadband moth-eye antireflection coatings on silicon.
9 *Appl. Phys. Lett.* **2008**, *92*, 061112.

10
11 (18) Yang, Z. P.; Ci, L. J.; Bur, J. A.; Lin, S. Y.; Ajayan, P. M., Experimental observation of
12 an extremely dark material made by a low-density nanotube array. *Nano Lett.* **2008**, *8*, 446-
13 451.

14
15 (19) Zhu, J. Y.; Yang, X.; Fu, Z. B.; Wang, C. Y.; Wu, W. D.; Zhang, L., Facile fabrication
16 of ultra-low density, high-surface-area, broadband antireflective carbon aerogels as ultra-black
17 materials. *J. Porous. Mat.* **2016**, *23*, 1217-1225.

18
19 (20) Sun, W.; Du, A.; Feng, Y.; Shen, J.; Huang, S. M.; Tang, J.; Zhou, B., Super Black
20 Material from Low-Density Carbon Aerogels With Subwavelength Structures. *ACS Nano*
21 **2016**, *10*, 9123-9128.

22
23 (21) Panagiotopoulos, N. T.; Diamanti, E. K.; Koutsokeras, L. E.; Baikousi, M.; Kordatos,
24 E.; Matikas, T. E.; Gournis, D.; Patsalas, P., Nanocomposite Catalysts Producing Durable,
25 Super-Black Carbon Nanotube Systems: Applications in Solar Thermal Harvesting. *ACS*
26 *Nano* **2012**, *6*, 10475-10485.

27
28 (22) Han, Z. W.; Wang, Z.; Li, B.; Feng, X. M.; Jiao, Z. B.; Zhang, J. Q.; Zhao, J.; Niu, S. C.;
29 Ren, L. Q., Flexible Self-Cleaning Broadband Antireflective Film Inspired by the Transparent
30 Cicada Wings. *Acs Appl. Mater. Inter.* **2019**, *11*, 17019-17027.

31
32 (23) Ghai, V.; Singh, H.; Agnihotri, P. K., Ultra-black superhydrophobic multilayer
33 broadband optical absorber. *MRS Adv.* **2019**, *4*(3-4), 163-168.

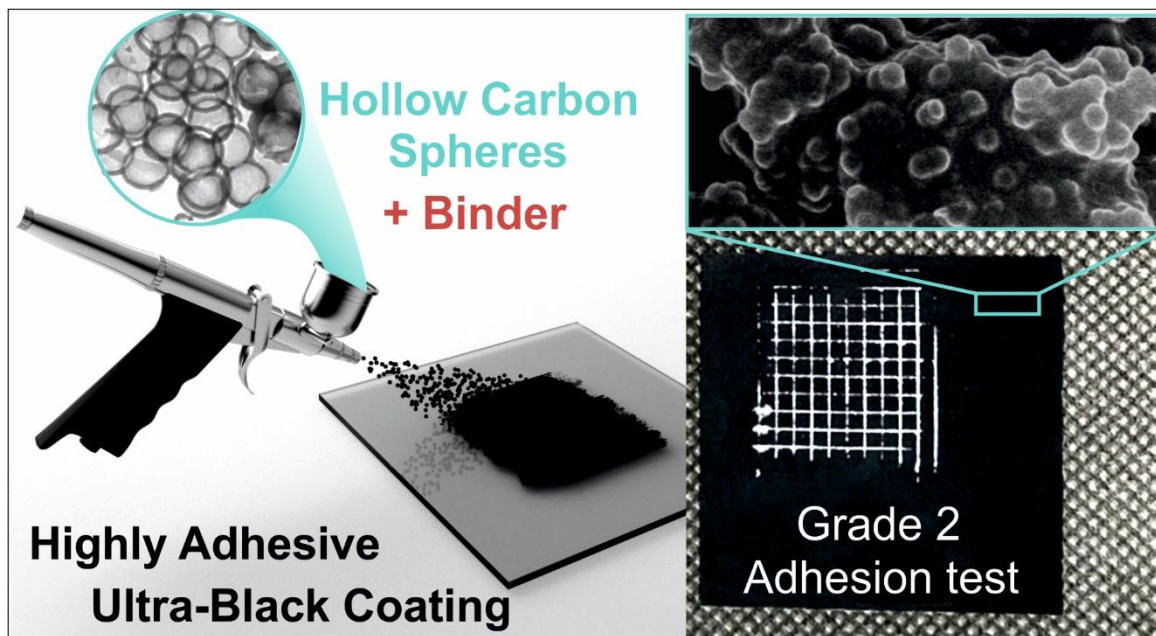
34
35 (24) Zhou, L.; Tan, Y. L.; Wang, J. Y.; Xu, W. C.; Yuan, Y.; Cai, W. S.; Zhu, S. N.; Zhu, J.,
36 3D self-assembly of aluminium nanoparticles for plasmon-enhanced solar desalination. *Nat.*
37 *Photonics* **2016**, *10*, 393.

38
39 (25) Zograf, G. P.; Petrov, M. I.; Zuev, D. A.; Dmitriev, P. A.; Milichko, V. A.; Makarov, S.
40 V.; Belov, P. A., Resonant Nonplasmonic Nanoparticles for Efficient Temperature-Feedback
41 Optical Heating. *Nano Lett.* **2017**, *17*, 2945-2952.

42
43 (26) Chen, X. B.; Liu, L.; Huang, F. Q., Black titanium dioxide (TiO₂) nanomaterials (vol 44,
44 pg 1861, 2015). *Chem. Soc. Rev.* **2015**, *44*, 2019-2019.

- 1
2
3
4 (27) Sheverdin, A.; Valagiannopoulos, C., Core-shell nanospheres under visible light:
5 Optimal absorption, scattering, and cloaking. *Phys. Rev. B* **2019**, 99,075305..
6
7 (28) Azoubel, S.; Cohen, R.; Magdassi, S., Wet deposition of carbon nanotube black coatings
8 for stray light reduction in optical systems. *Surf. Coat. Tech.* **2015**, 262, 21-25.
9
10 (29) Bera, R. K.; Mhaisalkar, S. G.; Mandler, D.; Magdassi, S., Formation and performance
11 of highly absorbing solar thermal coating based on carbon nanotubes and boehmite. *Energ.*
12 *Convers. Manage.* **2016**, 120, 287-293.
13
14 (30) Vinetsky, Y.; Jambu, J.; Mandler, D.; Magdassi, S., CNT-Based Solar Thermal
15 Coatings: Absorptance vs. Emittance. *Coatings* **2020**, 10 (11).
16
17 (31) Xu, J.; Shi, Y.; Li, J.; Cui, G.; Gu, G., Carbon Aerogel Based Waterborne Ultra-Black
18 Coatings with High Light Absorption. *Coatings* **2021**, 11 (5).
19
20 (32) Bychanok, D.; Li, S.; Sanchez-Sanchez, A.; Gorokhov, G., Kuzhir, P., Ogrin, F. Y.,
21 Pasc, A.; Ballweg, T.; Mandel, K.; Szczurek, A.; Fierro, V.; Celzard, A., Hollow carbon
22 spheres in microwaves: bio inspired absorbing coating. *Appl. Phys. Lett.* **2016**, 108, 013701.
23
24 (33) Pan, L.; Wang, Y.; Xu, H. B.; Ding, Y. B.; Li, Y.; Zhao, J. P., Synthesis of Silica
25 Particles with Precisely Tailored Diameter. *Chinese. J. Chem. Phys.* **2014**, 27, 563-567.
26
27 (34) Li, N.; Zhang, Q.; Liu, J.; Joo, J.; Lee, A.; Gan, Y.; Yin, Y. D., Sol-gel coating of
28 inorganic nanostructures with resorcinol-formaldehyde resin. *Chem. Commun.* **2013**, 49,
29 5135-5137.
30
31 (35) Gil-Herrera, L. K.; Blanco, A.; Juarez, B. H.; Lopez, C., Seeded Synthesis of
32 Monodisperse Core-Shell and Hollow Carbon Spheres. *Small* **2016**, 12, 4357-4362.
33
34 (36) Jiang, Q. S.; Li, C.; Shi, S. G.; Zhao, D. G.; Xiong, L.; Wei, H. L.; Yi, L., Assembling
35 ultra-thick and crack-free colloidal crystals via an isothermal heating evaporation induced self-
36 assembly method. *J. Non-Cryst. Solids* **2012**, 358, 1611-1616.
37
38 (37) Guo, J.; Li, D.; Qian, Z.; Luo, H.; Yang, M.; Wang, Q.; Xu, J.; Zhao, N., Carbon
39 Vesicles: A Symmetry-Breaking Strategy for Wide-Band and Solvent-Processable Ultrablack
40 Coating Materials. *Adv. Funct. Mater.* **2020**, 30, 1909877.
41
42 (38) Valagiannopoulos, C. A.; Alitalo, P., Electromagnetic cloaking of cylindrical objects by
43 multilayer or uniform dielectric claddings. *Phys. Rev. B* **2012**, 85 (11).
44
45
46
47
48
49
50
51
52
53
54
55

56 **ToC Figure**
57
58
59
60



1
2
3
4
5
6
7
8
9
10
11
12
13
14
15
16
17
18
19
20
21
22
23
24
25
26
27
28
29
30
31
32
33
34
35
36
37
38
39
40
41
42
43
44
45
46
47
48
49
50
51
52
53
54
55
56
57
58
59
60